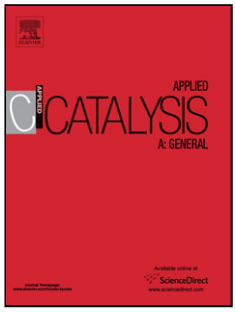

Ultrafine Ru nanoparticles anchored to porous g-C_3N_4 as efficient catalysts for ammonia borane hydrolysis

Yong-Ting Li (Methodology) (Investigation) (Writing - original draft), Shi-Hao Zhang (Methodology), Guang-Ping Zheng (Formal analysis) (Writing - review and editing), Pu Liu (Formal analysis) (Investigation), Zhi-Kun Peng (Formal analysis) (Conceptualization), Xiu-Cheng Zheng (Supervision) (Conceptualization) (Writing - review and editing)

PII: S0926-860X(20)30104-6

DOI: https://doi.org/10.1016/j.apcata.2020.117511

Reference: APCATA 117511

To appear in: *Applied Catalysis A, General*

Received Date: 2 December 2019

Revised Date: 28 January 2020

Accepted Date: 3 March 2020

Please cite this article as: Li Y-Ting, Zhang S-Hao, Zheng G-Ping, Liu P, Peng Z-Kun, Zheng X-Cheng, Ultrafine Ru nanoparticles anchored to porous g-C_3N_4 as efficient catalysts for ammonia borane hydrolysis, *Applied Catalysis A, General* (2020), doi: https://doi.org/10.1016/j.apcata.2020.117511

Ultrafine Ru nanoparticles anchored to porous g-C_3N_4 as efficient catalysts for ammonia borane hydrolysis

Yong-Ting Li[a], Shi-Hao Zhang[a], Guang-Ping Zheng[b], Pu Liu[a], Zhi-Kun Peng[c]*, Xiu-Cheng Zheng[a, d]*

[a] Green Catalysis Center, and College of Chemistry, Zhengzhou University, Zhengzhou 450001, China

[b] Department of Mechanical Engineering, The Hong Kong Polytechnic University, Hung Hom, Kowloon, Hong Kong, China

[c] Henan Institutes of Advanced Technology, Zhengzhou University, Zhengzhou 450003, China

[d] Key Laboratory of Advanced Energy Materials Chemistry (Ministry of Education), College of Chemistry, Nankai University, Tianjin 300071, China

*Corresponding author: E-mail address: zhxch@zzu.edu.cn (XCZ), pengzhikun@zzu.edu.cn (ZKP).

Graphical abstract

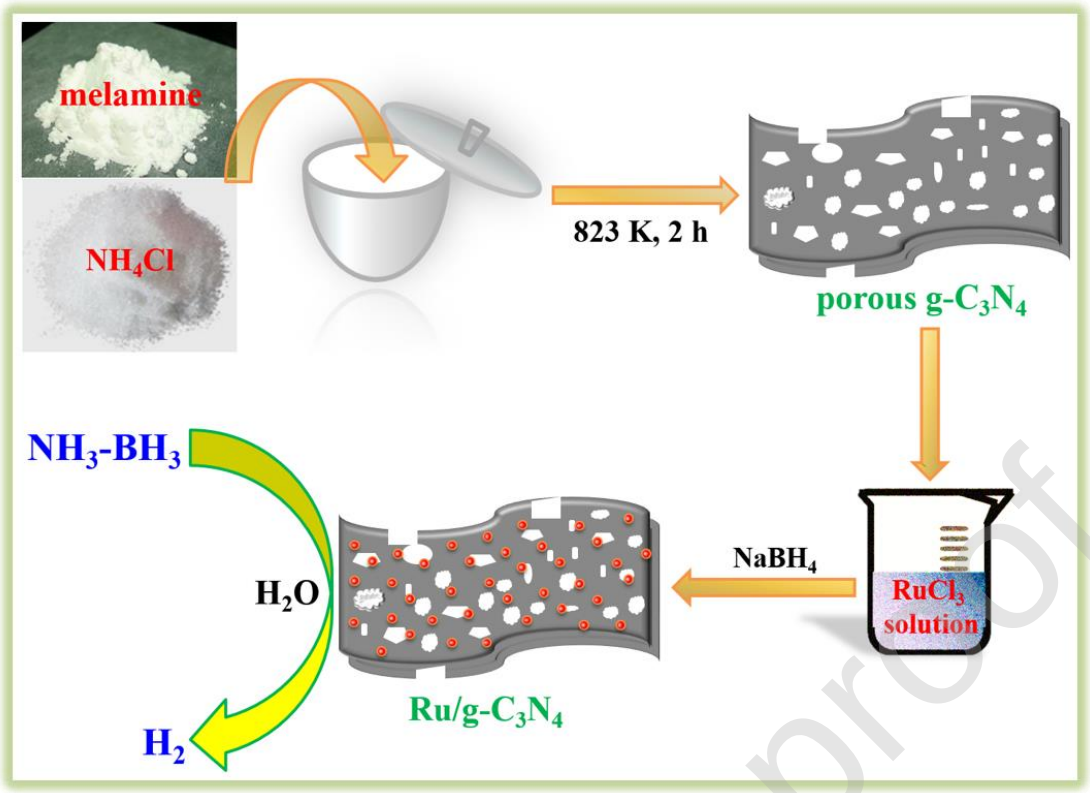

Highlights

- Porous g-C_3N_4 is facilely prepared from melamine using NH_4Cl as dynamic gas templates.
- g-C_3N_4 are used to evenly anchor the ultrafine Ru NPs for ammonia borane hydrolysis.
- The porous catalysts possess high catalytic activity and satisfactory recyclability.

Abstract: Hierarchical porous g-C_3N_4 nanosheets are prepared from melamine using NH_4Cl as dynamic gas templates to anchor the ultrafine Ru nanoparticles (NPs) with a

facile adsorption-*in situ* reduction strategy. The results reveal that 1 : 3 is the optimal mass ratio for melamine to NH_4Cl and the Ru NPs are evenly dispersed in the porous network of g-C_3N_4 in the corresponding catalysts. Remarkably, the porous catalysts exhibit superior catalytic activity and satisfactory recyclability for ammonia borane (NH_3-BH_3, AB) hydrolysis. The corresponding turnover frequency is as high as 122.2 × 10^3 $mL_{H_2} \cdot g_{Ru}^{-1} \cdot min^{-1}$ and the apparent activation energy (35.6 kJ mol^{-1}) is competitive. AB hydrolysis is of 1.17-order and near zero-order with respect to the Ru and AB concentrations, respectively. The results demonstrate that the Ru/g-C_3N_4 catalysts are promising in developing an alternative clean and environmentally friendly energy carrier from the hydrogen storage materials.

Keywords: g-C_3N_4; hierarchical porous structure; Ru nanoparticle; hydrogen; ammonia borane; hydrolysis.

1. Introduction

With the fast development of human society, more and more fossil fuels are being consumed, which may lead to possible energy crisis and serious environmental pollution. As a result, it is urgent to search for alternative energy sources [1]. Fortunately, hydrogen (H_2) has been recognized as an ultimate energy carrier because of its high energy capacity, abundance, and environmental friendliness [2, 3]. However, the controllable storage, safe delivery and efficient release of H_2 are still difficult to implement, which limit its widespread utilization. Thus, the development of suitable catalysts for H_2 generation from hydrogen storage materials under mild reaction conditions is crucial for the upcoming hydrogen-energy economy [4].

Among various chemical H_2 storage materials, ammonia borane (NH_3-BH_3, AB) is thought to be the most promising one due to its unique properties including high H_2

content (19.6 wt%), low molecular weight (30.87 g mol^{-1}), nontoxicity, and superior stability, etc. [5, 6]. Generally, H_2 generation from AB can take place by the pyrolysis or hydrolysis procedures and the latter is more attractive and facile since it can occur at ambient temperature. Three moles of H_2 may generate from one mole of AB in the hydrolysis reaction catalyzed by suitable catalysts, as described by (*Eq.* 1) [7]. In this reaction, catalysts are usually the pristine metal nanoparticles (NPs) or their supported ones, such as nanoporous Ru NPs [2], Pt/Ni [3], Ru/C [5], Rh/g-C_3N_4 [8], Rh/PPC [9], Rh/C-SC [10], Pt/CCF [11], Pd/PDA-$CoFe_2O_4$ [12], Ni@ZIF-8 [13], Ru@Co/CCF [1], CoRh/N-C [14], CoRh@ZIF-67 [15], Ni_2Pt@ZIF-8 [16], PtRu/CNT [17], AgCo/g-C_3N_4 [18], and CuCo/BN [19]. In particular, the supported Ru NPs are of much interest because of their superior catalytic performance and their low-cost in comparison with other noble metals [4, 5, 20-28].

$$NH_3BH_3\ (aq) + 2H_2O\ (l) \xrightarrow{\text{catalyst}} NH_4BO_2\ (aq) + 3H_2\ (g) \qquad (1)$$

Graphitic carbon nitride (g-C_3N_4), which may be easily prepared from various organic precursors by using the thermal polymerization method, possesses unique properties including excellent thermal and chemical stabilities, good visible light absorption and mild band gap (2.7 eV) because of its tris-triazine ring structure [29, 30]. These properties endow g-C_3N_4 promising applications in many fields such as photocatalysis and heterogeneous catalysis. In particular, the Ru NPs composited with g-C_3N_4 has aroused tremendous attention in recent years. For example, Navlani-García *et al.* [31] ascribed the enhanced performance of Ru/C/g-C_3N_4 in the AB dehydrogenation reaction to the additions of carbon, which dispersed and stabilized the small Ru NPs and enhances the optical absorption properties. Sharma and Sasson [32] found their Ru-g-C_3N_4 exhibited excellent catalytic performance for the hydrogen transfer reaction of aldehydes and ketone irradiated by visible light.

However, the disadvantages of using bulk g-C_3N_4, such as low surface area, low quantum efficiency caused by large grain size and severe agglomeration, have restrict its performance. Thus, it is necessary to adjust the microstructure of g-C_3N_4 to further enhance the catalytic performance of the corresponding catalysts.

Recently, Tian *et al.* [33] synthesized g-C_3N_4 with a mesoporous structure by using colloidal silica as templates to support the isolated single-atom Ru. The resulting Ru1/mpg-g-C_3N_4 showed excellent hydrogenation and hydride oxygenation performance in the conversion of biomass molecules. Compared to the conventional strategies of using soft and hard templates, the dynamic gas template method is cost-effective, non-toxic, and direct without any additional post-treatment [34].

Inspired by the aforementioned insights, we, herein, adopt a facile thermal decomposition approach to prepare hierarchical porous g-C_3N_4 from melamine by using ammonium chloride (NH_4Cl) as a dynamic gas template. Then, the ultrafine Ru NPs are encapsulated into the network of the resulting g-C_3N_4 by the adsorption-*in situ* reduction of $RuCl_3$ with $NaBH_4$. The structural characteristics of the novel Ru/g-C_3N_4 porous catalysts are verified with various techniques. The influence of different NH_4Cl dosages on the catalytic performance of the corresponding catalysts for AB hydrolysis is investigated to determine the most suitable g-C_3N_4 supports. The corresponding reaction kinetics is studied and the recyclability of the catalysts is verified. Also, the enhance effect of the NaOH addition on the catalysis efficiency is verified. The results demonstrate the as-prepared Ru/g-C_3N_4 are promising catalysts for H_2 generation from AB hydrolysis.

2. Experimental

2.1. *Materials*

Melamine (Sinopharm Chemical Reagent Co., Ltd), ammonium chloride (NH_4Cl,

Tianjin Fengchuan Chemical Reagent Co., Ltd), ruthenium(III) chloride ($RuCl_3 \cdot nH_2O$, Aladdin), hydrochloric acid (HCl, Luoyang Chemical Reagent Factory), ammonia borane (AB, 97%, Aladdin), and sodium borohydride ($NaBH_4$, 98%, Tianjin Tianli Chemical Reagent Co.) were of AR grade and used as received.

2.2. *Preparation of the Ru/g-C_3N_4 porous catalysts*

Porous g-C_3N_4 nanosheets were prepared from melamine with a thermal decomposition method using NH_4Cl as a dynamic gas template [35]. In brief, 0.50 g of melamine were mixed with certain amounts of NH_4Cl (0, 0.50, 1.00, 1.50, and 1.75 g), respectively, and ground evenly in an agate mortar. Then, the mixed solids were placed into a 100 mL crucible and calcined at 823 K for 2 h in a muffle furnace under air atmosphere (4 K min^{-1}). In this procedure, with gradually increasing calcination temperature, melamine was transferred to g-C_3N_4 and NH_4Cl decomposed to NH_3 and HCl gases, which played a significant role in the *in-situ* formation of porous g-C_3N_4 nanosheets [36, 37]. Unless otherwise specified, g-C_3N_4 cited in this work were the optimal one fabricated with a mass ratio of 1 : 3 for melamine to NH_4Cl.

The porous g-C_3N_4 was further used to anchor Ru NPs with an adsorption-*in situ* reduction method. Firstly, 1.0 L of HCl aqueous solution (pH = 2 ~ 3) was used to dissolve $RuCl_3 \cdot nH_2O$ solids (1.0 g), in which the exact content of Ru element was 0.4 mg mL^{-1} determined by inductively coupled plasma (ICP) analysis. Secondly, 17.7 mL of the aforementioned $RuCl_3$ solution was diluted with 20.0 mL of HCl solution (pH = 2 ~ 3), dispersed into 0.30 g of the as-prepared g-C_3N_4. After stirring for 12 h, the pH was adjusted to 6~7 with NaOH solution (1.0 mol L^{-1}). Thirdly, 10.0 mL of $NaBH_4$ solution with a molar ratio of 10 : 1 for $NaBH_4$ to $RuCl_3$ was added and kept stirring for 12 h. Finally, the solids were filtered, washed with deionized (DI) until the pH value became 7, and freeze-dried. The Ru loading was 0.189 mmol g^{-1} (1.91 wt%)

in the resultant Ru/g-C_3N_4 porous catalysts as calculated from the ICP analysis.

Also, g-C_3N_4 prepared with other mass ratios for melamine to NH_4Cl were used to anchor Ru NPs with the same loading applied through the synthesis procedure as mentioned above.

2.3. *Characterization*

The as-prepared materials were analyzed by transmission electron microscopy (TEM, TECNAIG^2F20-S-TWINJ transmission electron microscope), scanning electron microscopy (SEM, Sigma 500 field emission scanning electron microscope), X-ray diffraction (XRD, Panalytical XPert-Pro diffractometer, Cu K_a radiation, $\lambda = 0.154$ nm), N_2 adsorption-desorption (Micromeritics ASAP 2420-4MP automated surface area and pore size analyzer), inductively coupled plasma optical emission spectrometry (ICP-OES, 213DFG/ICPE-9820 Shimadzu multitype ICP emission spectrometer), and X-ray photoelectron spectroscopy (XPS, Shimadzu AXIS-UL TRA DLD XPS spectrometer).

2.4. *AB hydrolysis*

Before investigating the catalytic properties, the trace amount of Ru^{n+} species in the resulting catalysts were pre-reduced with AB as follows: Certain amount of catalysts and 10.0 mg of AB were placed into a round-bottomed flask (50 mL) equipped with a magnetic stirrer-oil bath system. Then, 15.0 mL of DI water was poured into the reactor immediately under stirring at 303 K. The excessive AB was hydrolyzed to generate H_2. Then, certain amount of AB dissolved into 10.0 mL of DI water was added. The hydrogen volume generated was measured by a water replacement method [7]. In order to remove the possible by-products (such as NH_3 come from *Eq.* 2), the generated gases were pretreated with HCl aqueous solution (0.2 M, 150 mL) in a 250 mL gas washing bottle before entering the capacity tube.

$$NH_3BH_3\ (aq) + NaOH\ (aq) + H_2O\ (l) \xrightarrow{\text{catalyst}} NaBO_2\ (aq) + NH_3\ (g) + 3H_2\ (g) \quad (2)$$

Firstly, the influence of different mass ratios of melamine to NH_4Cl on AB hydrolysis was investigated under the reaction conditions of catalyst dosage 25.0 mg and AB dosage 31.0 mg.

Secondly, in order to verify the reaction kinetics of AB hydrolysis over the Ru/g-C_3N_4 porous catalysts, a series of catalytic experiments were performed by altering the catalyst dosage (5.0-25.0 mg) with the AB dosage of 31.0 mg, the AB amount (0.25-1.00 mmol) with the catalyst dosage of 10.0 mg, and the temperature (303-318 K) with an AB dosage of 31.0 mg and a catalyst amount of 10.0 mg, respectively.

Thirdly, the recyclability of Ru/g-C_3N_4 was evaluated under the reaction conditions of AB dosage of 31.0 mg, catalyst amount of 10.0 mg, and reaction temperature of 303 K. Once completing a hydrolysis run, same amount (31.0 mg) of AB was supplemented to start the next cycle.

Finally, the influence of different dosages of NaOH on AB hydrolysis was investigated under the reaction conditions of AB dosage of 31.0 mg, catalyst amount of 10.0 mg, and reaction temperature of 303 K.

The corresponding apparent activation energy (E_a) was calculated with *Eq.* 3 [7].

$$\ln rate = -\left(\frac{E_a}{RT}\right) + C \ , \quad (3)$$

where T was the operating hydrolysis temperature (K), R was the molar gas constant (8.314 J $mol^{-1}\cdot K^{-1}$), and C was the corresponding constant.

The turnover frequency (TOF) was calculated with *Eq.* 4.

$$TOF = \frac{V_{H_2}}{t \times m_{Ru}} \ , \quad (4)$$

where V_{H_2} was the hydrogen amount generated (mL), t was the corresponding

hydrolysis time (min), and m_{Ru} was the amount of Ru in the Ru/g-C_3N_4 catalysts acquitted from the catalyst dosage and the aforementioned ICP analysis result (g).

3. Results and discussion

The XRD patterns shown in Fig. 1a demonstrate Ru/g-C_3N_4 maintains the crystal characteristic of pristine porous g-C_3N_4. The weak peak appeared at 13.3° and the strong one situated at 27.0° are ascribed to the (100) and (002) planes of g-C_3N_4, respectively. The former is assigned to the intra-planar repeating tri-s-triazine ring structure, and the latter is attributed to the inter-planar stacking of the conjugated aromatic structure [8]. Meanwhile, the characteristic peaks of Ru crystals are not visible in the pattern of Ru/g-C_3N_4 [31], which is presumably ascribed to the small particle size, low loading and high dispersion degree of Ru NPs in the catalysts.

The Ru/g-C_3N_4 porous catalysts are characterized by both SEM and TEM analyses to explore their detailed structural information. The SEM image shown in Fig. 2a verifies that abundant macropores appear in the g-C_3N_4 sheets, which are created by the volatilizations of NH_3 and HCl gases come from the decomposition of NH_4Cl. The porous structure also can be found in the TEM images (Fig. 2b and c). Meanwhile, as illustrated in Fig. 2b and c, it is noteworthy that no obvious aggregation for Ru NPs occurs in the Ru/g-C_3N_4 catalysts. The corresponding Ru particle size histogram shows a range of 1.9-5.1 nm and suggests that those NPs with a size of 2.7 nm possess the largest fraction (inset of Fig. 2c). In our opinion, the hierarchal porous structure with enlarged specific surface area, which is further confirmed in the subsequent N_2 adsorption-desorption analysis, endows the resulting g-C_3N_4 high adsorption capacity for $RuCl_3$ in the precursor solution. During the subsequent adsorption-*in situ* reduction procedure, the ambient reaction temperature

(room temperature), the violent stirring, and the suitable reaction speed facilitate the conversion of the encapsulated $RuCl_3$ species to metallic Ru with high dispersion degree by using $NaBH_4$ as reducing agent. Also, they effectively suppress the further aggregation of Ru NPs, forming the small Ru nanoparticles. The highly dispersed Ru NPs with such small sizes in the network of g-C_3N_4 endow Ru/g-C_3N_4 enough active sites, which could enhance their catalytic performance. The high-resolution TEM (HRTEM) image is shown in Fig. 2d. On the one hand, the HRTEM image displays the isolated Ru NPs anchored to g-C_3N_4, further indicating their features of high dispersion degree. On the other hand, obvious lattice lines are visible in the HRTEM image, which are attributed to the corresponding planes of g-C_3N_4 and Ru. For example, the worm lattice fringes are belonging to the (002) plane of g-C_3N_4, while those with a lattice spacing of 0.206 nm are attributed to the (101) plane of Ru [38]. The EDX elemental mapping shown in Fig. 3 evidences the existence of Ru, C and N elements in the Ru/g-C_3N_4 porous catalysts. Also, the Ru elemental mapping further verifies the uniform dispersion of Ru NPs in the catalysts.

The surface composition of the Ru/g-C_3N_4 porous catalysts is determined by XPS characterization (Fig. 4). The XPS signals corresponding to the elements of Ru, C, N, and O appear in the survey spectrum (Fig. 4a), indicating the successful anchoring of Ru to g-C_3N_4. In order to further detect the chemical interactions among these elements, XPS deconvolution spectra of the corresponding binding energy regions for C are recorded. For the C 1s spectra partially overlapped by those of Ru 3d, as shown in Fig. 4b, the divided peaks at 285.8, 284.8, 282.9 and 280.7 eV are attributed to N-C=N, C-C, Ru^0 $3d_{3/2}$, and Ru^0 $3d_{5/2}$, respectively [22, 24]. The presence of Ru^0 species confirms the successful reduction of $RuCl_3$ with $NaBH_4$ to form Ru NPs. Meanwhile, the other two divided peaks appear at 284.3 and 281.5 eV,

which are consistence with Ru^{n+} $3d_{3/2}$ and Ru^{n+} $3d_{5/2}$, respectively [21]. The formation of Ru^{n+} species presumably occurs within the sample preparation procedure for XPS measurements, which is similar to those of Ru/HfO_2 [27] and Ru/graphene [39], or might result from the oxidation of a part of Ru NPs exposed in air. The Ru 3p spectra shown in Fig. 4c further confirm the existence of Ru NPs in the Ru/g-C_3N_4 porous catalysts. In addition, the binding energy of the Ru^0 $3p_{3/2}$ level (462.5 eV) is lower than that of pure Ru [20] because of the strong interaction between Ru NPs and g-C_3N_4. The N 1s spectrum is divided into three peaks (Fig. 4d). The one at 399.0 eV is attributed to the sp^2-bonded N in the tri-s-triazine units (C=N-C). The one appeared at 400.4 eV is related to the bridging nitrogen atoms in $(C)_3$-N, and the one at 401.7 eV is assigned to the nitrogen atoms bonded with hydrogen atoms (C-NH_x) [32, 37].

The N_2 adsorption-desorption analysis is performed to verify the porous characteristics of Ru/g-C_3N_4 (Fig. 5). The isotherm shown in Fig. 5a reveals that no obvious nitrogen uptake change appears in low relative pressure range ($P/P_0 < 0.15$), indicating the scarcity of micropores in the catalysts. A hysteresis loop appears in the P/P_0 range of 0.45-1.00, verifying the existence of mesopores and macropores [40]. The specific surface area and total pore volume are 45.4 $m^2 g^{-1}$ and 0.254 $cm^3 g^{-1}$, respectively. While the adsorption average pore width (D_{a1}), Barrett-Joyner-Halenda (BJH) adsorption average pore diameter (D_{a2}) and BJH desorption average pore diameter (D_{a3}) are 22.4, 17.4 and 15.0 nm, respectively. The corresponding pore size distribution curves are obtained from both branches of adsorption and desorption by the density functional theory (DFT) model and BJH method, respectively (Fig. 5b-f). All the curves further demonstrate the catalysts possess well-developed meso- and macro-pores. Such hierarchical porous structure leads to the increased surface-active sites and diffusion channels for the mass transfer of reactant (AB) and product (H_2)

molecules, benefiting the catalytic performance when used as catalysts.

As mentioned above, the NH_3 and HCl gases, which are produced from the decomposition of NH_4Cl, volatilize during the calcination procedure accompanying the conversion of melamine to g-C_3N_4. Correspondingly, the sheets of g-C_3N_4 are stripped to have a reduced thickness and pores are left in the sheets. That's to say, NH_4Cl acts a key role in regulating the porous structure of g-C_3N_4. Considering the fact that the catalysis is shape selective, it is necessary to optimize the mass ratio of melamine to NH_4Cl. Fig. 6 shows the influence of different mass ratios on the catalytic activity of the corresponding Ru/g-C_3N_4 catalysts for AB hydrolysis. We can see that the catalysts prepared without the usage of NH_4Cl, which is denoted as $m_{\text{melamine}} : m_{\text{ammonium chloride}} = 1 : 0$ in Fig. 6, exhibit much lower catalytic activity than other catalysts, indicating the gas template offer positive effect for enhancing the catalytic activity. Furthermore, the H_2 generation *rate* increases with the decrease of the mass ratios and the catalysts corresponding to the ratio of 1 : 3 possess the highest catalytic activity under the present conditions. When further increasing the ratio to 1 : 3.5, the corresponding catalysts offer lower reaction *rate* than that with the aforementioned mass ratio (1 : 3). Fig. S1 in Supplementary Material shows the N_2 adsorption-desorption isotherms and pore size distribution curves of the resulting g-C_3N_4 prepared with different mass ratios of melamine to NH_4Cl. Table 1 in Supplementary Material shows their corresponding porous characteristics. As shown in Fig. S1 and Table 1, compared with the bulk g-C_3N_4 ($S_{Langmuir}$ = 7.6 $m^2\ g^{-1}$, S_{BET} = 5.3 $m^2\ g^{-1}$, V_p = 0.026 $cm^3\ g^{-1}$), the resulting porous g-C_3N_4 prepared using NH_4Cl possess higher surface area and larger pore volume. Among them, the one prepared with the mass ratio of 1 : 3 exhibits the highest surface area ($S_{Langmuir}$ = 82.9 $m^2\ g^{-1}$, S_{BET} = 59.1 $m^2\ g^{-1}$), largest total pore volume (0.317 $cm^3\ g^{-1}$) and the most abundant

meso- and macro-pores. The different porous parameters affect the dispersion degree and particle size of the Ru NPs when used as supports, leading to the difference in catalytic activities. Therefore, 1 : 3 is the optimal mass ratio of melamine to NH_4Cl under the present conditions to synthesize porous g-C_3N_4. We choose the corresponding Ru/g-C_3N_4 for the subsequent studies on the reaction kinetics.

Firstly, the influences of different Ru/g-C_3N_4 dosages on the H_2 generation *rate* are investigated. As illustrated in Fig. 7a, the AB hydrolysis *rate* increases continuously with increasing catalyst dosage. The catalytic reaction is completed within 30.0, 12.0, 10.5, 7.5 and 6.0 minutes when the Ru/g-C_3N_4 dosage is 5.0, 10.0. 15.0, 20.0 and 25.0 mg, respectively. It could be due to the fact that the added catalysts increase the total number of active sites for AB hydrolysis. Meanwhile, the corresponding TOF values for the aforementioned cases are 33.0×10^3, 42.1×10^3, 28.5×10^3, 30.7×10^3 and 35.0×10^3 $mL_{H_2} \cdot g_{Ru}^{-1} \cdot min^{-1}$, respectively. Therefore, the Ru/g-C_3N_4 dosage of 10.0 mg is adopted in the following kinetics study. The plots of ln *rate* versus ln [Ru] shown in Fig. 7b are fitted with a straight line owning a slope of 1.17, verifying AB hydrolysis is of 1.17-order with respect to Ru concentration under the present conditions, i.e., the AB dosage 31.0 mg, DI water 25.0 mL, and reaction temperature 303 K.

Secondly, a series of hydrolysis reactions with different AB dosages catalyzed by Ru/g-C_3N_4 are performed. As shown in Fig. 8a, the H_2 volume generated increases with the increase of AB dosage. The corresponding TOF values are 25.4×10^3, 28.4×10^3, 34.7×10^3 and 42.1×10^3 $mL_{H_2} \cdot g_{Ru}^{-1} \cdot min^{-1}$ when the AB dosages are 0.25, 0.50, 0.75 and 1.00 mmol, respectively. The plots of ln *rate* versus ln [AB] shown in Fig. 8b

are fitted with a straight line owning a slope of 0.06, verifying that the hydrolysis is of near zero-order with respect to the AB concentration under the present conditions, i.e., the catalyst dosage 10.0 mg, DI water 25.0 mL, and reaction temperature 303 K.

Thirdly, the hydrolysis reaction catalyzed by Ru/g-C_3N_4 is further carried out at different temperatures (303, 308, 313, and 318 K). The H_2 generation *rate* increases with the increase of the hydrolysis temperature (Fig. 9a) since high temperature facilitates the effective collisions among the activated reactant molecules. Correspondingly, the TOF values are 42.1×10^3, 42.9×10^3, 45.4×10^3 and 70.0×10^3 $mL_{H_2} \cdot g_{Ru}^{-1} \cdot min^{-1}$, respectively. Fig. 9b gives the liner relation between ln *rate* and 10^3/T, which is fitted as $\ln rate = -\frac{4284.0}{T} + 15.90$. The corresponding E_a is 35.6 kJ mol^{-1} based on *Eq.* 2. As shown in Table 1, the as-prepared Ru/g-C_3N_4 possesses lower E_a than many Ru-based catalysts previously reported.

Finally, the recyclability experiments are performed under the conditions of catalyst dosage 10.0 mg, AB dosage 31.0 mg, DI water 25.0 mL, and reaction temperature 303 K. As shown in Fig. 10, although the Ru/g-C_3N_4 porous catalysts maintain stable activity, even in the fourth run, the reaction time of the 5th run is extended obviously. The TOF value decreases from 38.6×10^3 $mL_{H_2} \cdot g_{Ru}^{-1} \cdot min^{-1}$ for the first run to 26.0×10^3 $mL_{H_2} \cdot g_{Ru}^{-1} \cdot min^{-1}$ for the fifth run. On the one hand, the activity loss might be caused by the slight growth of Ru NPS. Fig. S2 in Supplementary Material shows the HRTEM images of the recycled Ru/g-C_3N_4 porous catalysts and the corresponding particle size distribution of Ru NPs. We can see that although the Ru NPs are still highly dispersed in g-C_3N_4, which is consistent with the

XRD analysis for the recycled Ru/g-C_3N_4 (Fig. S3 in Supplementary Material), their particle sizes distribute in the range of 2.4-6.0 nm and the 3.3 nm ones possessing the largest fraction. In other words, Ru NPs own slightly larger particle size in the recycled catalysts than in the fresh catalysts (insert of Fig. 2c). Similar results are also appeared in the case of Pd-based catalysts [47]. On the other hand, the increasing amounts of NH_4BO_2 produced also causes the activity loss. This is due to that these NH_4BO_2 species block the pores and occupy the active sites of the catalysts, result in the increased viscosity of the reaction system.

Wei *et al.* [14] found that the addition of NaOH can improve the catalytic activity of their CoRu@N-C catalysts for AB hydrolysis since the OH^- ions act as co-catalysts to active the water molecules. In order to further improve the catalysis efficiency, we investigate the influence of different NaOH dosages. As shown in Fig. S4 in Supplementary Material, compared with the original reaction in the absence of NaOH, the introducing of NaOH greatly accelerates the hydrolysis rate. Moreover, the activity increases with increasing NaOH dosage from 0.25 to 0.75 g. Correspondingly, the TOF increases from 78.1 × 10^3 to 122.2 × 10^3 $mL_{H_2} \cdot g_{Ru}^{-1} \cdot min^{-1}$. As illustrated in Table 1, this value (122.2 × 10^3 $mL_{H_2} \cdot g_{Ru}^{-1} \cdot min^{-1}$) is obviously larger than those of the Ru-based catalysts previously reported. When further increasing NaOH dosage to 1.00 g, the hydrolysis rate does not increase anymore. Even an opposite behavior appears and the corresponding TOF decreases to 116.6 × 10^3 $mL_{H_2} \cdot g_{Ru}^{-1} \cdot min^{-1}$. The favorable effect of NaOH is presumably originated from the coordination of OH^- ions to the Ru nanoparticle surface, endowing these NPs more electron-rich, which favors

the rate-limiting oxidative OH^- addition of water. Similar results have been found in the AB hydrolysis cases catalyzed by Ni_2Pt@ZIF-8 [16]. However, overmuch coordination may occupy the Ru surface active sites, partly inhibits the oxidative addition of the water O-H bond, leading to a decreased hydrolysis rate.

4. Conclusions

In summary, the hierarchal porous g-C_3N_4 sheets are prepared from melamine with a thermal polymerization method by using NH_4Cl. Furthermore, the resulting g-C_3N_4 is applied to evenly anchor ultrafine Ru nanoparticles to construct the Ru/g-C_3N_4 porous catalysts for AB hydrolysis. Wherein, the as-prepared catalysts possess high catalytic activity and satisfactory recyclability. The corresponding turn over frequency could reach up to 122.2 × 10^3 $mL_{H_2} \cdot g_{Ru}^{-1} \cdot min^{-1}$ in the presence of NaOH with the optimal amount (0.75 g) and the apparent activation energy is only 35.6 kJ mol^{-1}. The results reveal the Ru/g-C_3N_4 porous catalysts are promising for the hydrolytic dehydrogenation of hydrogen storage materials.

Credit Author Statement

Yong-Ting Li: Methodology, Investigation, Writing - original draft.

Shi-Hao Zhang: Methodology.

Guang-Ping Zheng: Formal analysis, Writing - review & editing.

Pu Liu: Formal analysis, Investigation.

Zhi-Kun Peng: Formal analysis, Conceptualization.

Xiu-Cheng Zheng: Supervision, Conceptualization, Writing - review & editing.

Acknowledgements

This study is supported by the National Natural Science Foundation of China (CN) (No. U1304203), the 111 Project (CN) (No. B12015), the Natural Science Foundation of Henan Province (CN) (No. 162300410258), and the National College Students Innovation and Entrepreneurship Training Program of China (CN) (No. 201910459081).

References

[1] J. Yang, Z.K. Cui, J.T. Ma, Z.P. Dong, Ru coated Co nanoparticles decorated on cotton derived carbon fibers as a highly efficient and magnetically recyclable catalyst for hydrogen generation from ammonia borane, Int. J. Hydrogen Energy 43 (2018) 1355–1364.

[2] Q.X. Zhou, H.X. Yang, C.X. Xu, Nanoporous Ru as highly efficient catalyst for hydrolysis of ammonia borane, Int. J. Hydrogen Energy 41 (2016) 12714–12721.

[3] Z. Li, T. He, D. Matsumura, S. Miao, A.A. Wu, L. Liu, G. Wu, P. Chen, Atomically dispersed Pt on the surface of Ni particles: synthesis and catalytic function in hydrogen generation from aqueous ammonia-borane, ACS Catal. 7 (2017) 6762–6769.

[4] K. Mori, K. Miyawaki, H. Yamashita, Ru and Ru-Ni nanoparticles on TiO_2 support as extremely active catalysts for hydrogen production from ammonia-borane, ACS Catal. 6 (2016) 3128−3135.

[5] M. Navlani-García, K. Mori, A. Nozaki, Y. Kuwahara, H. Yamashita, Highly efficient Ru/carbon catalysts prepared by pyrolysis of supported Ru complex towards the hydrogen production from ammonia borane, Appl. Catal. A: Gen. 527 (2016) 45–52.

[6] B. Qi, L.Y. Du, F.Z. Yao, S.R. Xu, X.F. Deng, M. Zheng, S.H. He, H.B. Zhang,

X.H. Zhou, Shape-controlled dodecaborate supramolecularorganic-framework-supported ultrafine trimetallic PtCoNi for catalytic hydrolysis of ammonia borane, ACS Appl. Mater. Interfaces 11 (2019) 23445–23453.

[7] S. Liu, X. Chen, Z.J. Wu, X.C. Zheng, Z.K. Peng, P. Liu, Chitosan-reduced graphene oxide hybrids encapsulated Pd(0) nanocatalysts for H_2 generation from ammonia borane, Int. J. Hydrogen Energy 44 (2019) 23610−23619.

[8] R. Lu, M. Hu, C.L. Xu, Y. Wang, Y. Zhang, B. Xu, D.J. Gao, J. Bi, G.Y. Fan, Hydrogen evolution from hydrolysis of ammonia borane catalyzed by Rh/g-C_3N_4 under mild conditions, Int. J. Hydrogen Energy 43 (2018) 7038−7045.

[9] H. Liu, C.L. Xu, R. Lu, Q. Wang, J. Wu, Y. Wang, Y. Zhang, T. Sun, G.Y. Fan, Efficient hydrogen evolution from ammonia borane hydrolysis with Rh decorated on phosphorus-doped carbon, Int. J. Hydrogen Energy 44 (2019) 16548−16556.

[10] J.Q. Chen, M. Hu, M. Ming, C.L. Xu, Y. Wang, Y. Zhang, J.T. Wu, D.J. Gao, J. Si, G.Y. Fan, Carbon-supported small Rh nanoparticles prepared with sodium citrate: toward high catalytic activity for hydrogen evolution from ammonia borane hydrolysis, Int. J. Hydrogen Energy 43 (2018) 2718−2725.

[11] M. Yuan, Z.K. Cui, J. Yang, X.L. Cui, M. Tian, D. Xu, J.T. Ma, Z.P. Dong, Ultrafine platinum nanoparticles modified on cotton derived carbon fibers as a highly efficient catalyst for hydrogen evolution from ammonia borane, Int. J. Hydrogen Energy 42 (2017) 29244−29253.

[12] J. Manna, S. Akbayrak, S. Özkar, Palladium(0) nanoparticles supported on polydopamine coated $CoFe_2O_4$ as highly active, magnetically isolable and reusable catalyst for hydrogen generation from the hydrolysis of ammonia borane, Appl. Catal. B: Environ. 208 (2017) 104−115.

[13] C.L. Wang, J. Tuninetti, Z. Wang, C. Zhang, R. Ciganda, L. Salmon, S. Moya, J. Ruiz, D. Astruc, Hydrolysis of ammonia borane over Ni/ZIF-8 nanocatalyst: high efficiency, mechanism, and controlled hydrogen release, J. Am. Chem. Soc. 139 (2017) 11610−11615.

[14] Z.H. Wei, Y. Liu, Z.K. Peng, H.Q. Song, Z.Y. Liu, B.Z. Liu, B.J. Li, B. Yang, S.Y. Lu, Cobalt-ruthenium nanoalloys parceled in porous nitrogen-doped graphene as highly efficient difunctional catalysts for hydrogen evolution reaction and hydrolysis of ammonia borane, ACS Sustainable Chem. Eng. 7 (2019) 7014−7023.

[15] X.P. Qu, Z.Q. Yu, Z.P. Li, X.Y. Gui, R. Jiang, Z.M. Xu, C.H. Chen, J. Peng, CoRh nanoparticles supported on ZIF-67 as highly efficient catalysts for hydrolytic dehydrogenation of ammonia boranes for chemical hydrogen storage, Int. J. Hydrogen Energy 42 (2017) 30037−30043.

[16] F.Y. Fu, C.L. Wang, Q. Wang, A.M. Martinez-Villacorta, A. Escobar, H.B. Chong, X. Wang, S. Moya, L. Salmon, E. Fouquet, J. Ruiz, D. Astruc, Highly selective and sharp volcano-type synergistic Ni_2Pt@ZIF-8-catalyzed hydrogen evolution from ammonia borane hydrolysis, J. Am. Chem. Soc. 140 (2018) 10034−10042.

[17] W.Y. Chen, D.L. Li, C. Peng, G. Qian, X.Z. Duan, D. Chen, X.G. Zhou, Mechanistic and kinetic insights into the Pt-Ru synergy during hydrogen generation from ammonia borane over PtRu/CNT nanocatalysts, J. Catal. 356 (2017) 186−196.

[18] Q. Wang, C.L. Xu, M. Ming, Y.C. Yang, B. Xu, Y. Wang, Y. Zhang, J. Wu, G.Y. Fan, In situ formation of AgCo stabilized on graphitic carbon nitride and concomitant hydrolysis of ammonia borane to hydrogen, Nanomaterials 8 (2018)

280.

[19] X. Yang, Q.L. Li, L.L. Li, J. Lin, X.J. Yang, C. Yu, Z.Y. Liu, Y. Fang, Y. Huang, C.C. Tang, CuCo binary metal nanoparticles supported on boron nitride nanofibers as highly efficient catalysts for hydrogen generation from hydrolysis of ammonia borane, J. Power Sources 431 (2019) 135−143.

[20] G.Y. Fan, Q.Q. Liu, D.M. Tang, X.J. Li, J. Bi, D.J. Gao, Nanodiamond supported Ru nanoparticles as an effective catalyst for hydrogen evolution from hydrolysis of ammonia borane, Int. J. Hydrogen Energy 41 (2016) 1542−1549.

[21] R.Y. Wang, Y. Wang, M.Q. Ren, G.X. Sun, D.W. Gao, Y.R.C. Chong, X. Li, GZ Chen, Effect of ceria morphology on the catalytic activity of Ru/ceria for the dehydrogenation of ammonia borane, Int. J. Hydrogen Energy 42 (2017) 6757−6764.

[22] F.Y. Zhong, Q. Wang, C.L. Xu, Y.C. Yang, Y. Wang, Y. Zhang, D.J. Gao, J. Bi, G.Y. Fan, Ultrafine and highly dispersed Ru nanoparticles supported on nitrogen doped carbon nanosheets: efficient catalysts for ammonia borane hydrolysis, Appl. Surf. Sci. 455 (2018) 326–332.

[23] K.Z. Yang, L.Q. Zhou, G.F. Yu, X. Xiong, M.L. Ye, Y. Li, D. Lu, Y.X. Pan, M.H. Chen, L. Zhang, D.D. Gao, Z. Wang, H.Y. Liu, Q.H. Xia, Ru nanoparticles supported on MIL-53(Cr, Al) as efficient catalysts for hydrogen generation from hydrolysis of ammonia borane, Int. J. Hydrogen Energy 41 (2016) 6300−6309.

[24] E. Sarıca, S. Akbayrak, S. Özkar, Ruthenium(0) nanoparticles supported on silica coated Fe_3O_4 as magnetically separable catalysts for hydrolytic dehydrogenation of ammonia borane, Int. J. Hydrogen Energy 43 (2018) 15124−15134.

[25] W. Zhao, R.Y. Wang, Y. Wang, J.W. Feng, C.C. Li, G.Z. Chen, Effect of LDH composition on the catalytic activity of Ru/LDH for the hydrolytic

dehydrogenation of ammonia borane, Int. J. Hydrogen Energy 44 (2019) 14820−14830.

[26] G.Z. Chen, R.Y. Wang, W. Zhao, B.T. Kang, D.W. Gao, C.C. Li, J.Y. Lee, Effect of Ru crystal phase on the catalytic activity of hydrolytic dehydrogenation of ammonia borane, J. Power Sources 396 (2018) 148–154.

[27] E.B. Kalkan, S. Akbayrak, S. Özkar, Ruthenium(0) nanoparticles supported on nanohafnia: a highly active and long-lived catalyst in hydrolytic dehydrogenation of ammonia borane, J. Mole. Catal. A: Chem. 430 (2017) 29–35.

[28] Z.J. Wu, Y.L. Duan, S.H. Ge, A.C.K. Yip, F. Yang, Y.F. Li, T. Dou, Promoting hydrolysis of ammonia borane over multiwalled carbon nanotube-supported Ru catalysts via hydrogen spillover, Catal. Commun. 91 (2017) 10–15.

[29] D. Huang, X. Yan, M. Yan, G. Zeng, C. Zhou, J. Wan, M. Cheng, W. Xue, Graphitic carbon nitride based heterojunction photoactive nanocomposites: applications and mechanism insight, ACS Appl. Mater. Interfaces 10 (2018) 21035–21055.

[30] M.A. Khan, M. Xia, S. Mutahir, T. Muhmood, W. Lei, F. Wang, Encapsulating nano rods of copper-biphenylamines framework on g-C_3N_4 photocatalysts for visible light-driven organic dyes degradation: promoting charge separation efficiency, Catal. Sci. Technol. 7 (2017) 3017–3026.

[31] M. Navlani-García, P. Verma, Y. Kuwahara, T. Kamegawa, K. Mori, H. Yamashita, Visible-light-enhanced catalytic activity of Ru nanoparticles over carbon modified g-C_3N_4, J. Photochem. Photobio. A 358 (2018) 327–333.

[32] P. Sharma, Y. Sasson, A photoactive catalyst Ru-g-C_3N_4 for hydrogen transfer reaction of aldehydes and ketones, Green Chem. 19 (2017) 844–852.

[33] S.B. Tian, Z.Y. Wang, W.B. Gong, W.X. Chen, Q.C. Feng, Q. Xu, C. Chen, C. Chen, Q. Peng, L. Gu, H.J. Zhao, P. Hu, D.S. Wang, Y.D. Li, Temperature-controlled selectivity of hydrogenation and hydrodeoxygenation in the conversion of biomass molecule by the Ru_1/mpg-C_3N_4 catalyst, J. Am. Chem. Soc. 140 (2018) 11161−11164.

[34] W. Iqbal, B. Yang, X. Zhao, M. Waqas, M. Rauf, C.Q. Guo, J.L. Zhang, Y.P. Mao, Gaseous bubble-assisted in-situ construction of worm-like porous g-C_3N_4 with superior visible light photocatalytic performance, Appl. Catal A: Gen. 573 (2019) 13–21.

[35] W. Iqbal, C.Y. Dong, M.Y. Xing, X.J. Tan, J.L. Zhang, Eco-friendly one-pot synthesis of well-adorned mesoporous g-C_3N_4 with efficiently enhanced visible light photocatalytic activity, Catal. Sci. Technol. 7 (2017) 1726–1734.

[36] B. Babu, J. Shim, A.N. Kadam, K. Yoo, Modification of porous g-C_3N_4 nanosheets for enhanced photocatalytic activity: in-situ synthesis and optimization of NH_4Cl quantity, Catal. Commun. 124 (2019) 123−127.

[37] D. Zhang, Y.L. Guo, Z.K. Zhao, Porous defect-modified graphitic carbon nitride via a facile one-step approach with significantly enhanced photocatalytic hydrogen evolution under visible light irradiation, Appl Catal B: Environ. 226 (2018) 1−9.

[38] N. Cao, J. Su, W. Luo, G.Z. Cheng, Hydrolytic dehydrogenation of ammonia borane and methylamine borane catalyzed by graphene supported Ru@Ni core-shell nanoparticles, Int. J. Hydrogen Energy 39 (2014) 426−435.

[39] N. Cao, W. Luo, G.Z. Cheng, One-step synthesis of graphene supported Ru nanoparticles as efficient catalysts for hydrolytic dehydrogenation of ammonia borane, Int. J. Hydrogen Energy 38 (2013) 11964−11972.

[40] T.T. Ma, X.H. Liu, L. Sun, Y.S. Xu, L.L. Zheng, J. Zhang, Strongly coupled N-doped carbon/Fe_3O_4/N-doped carbon hierarchical micro/nanostructures for enhanced lithium storage performance, J. Energy Chem. 34 (2019) 43−51.

[41] S. Basu, A. Brockman, P. Gagare, Y. Zheng, P.V. Ramachandran, W.N. Delgass, J.P. Gore, Chemical kinetics of Ru-catalyzed ammonia borane hydrolysis, J. Power Sources 188 (2009) 238−243.

[42] S. Akbayrak, S. Özkar, Ruthenium(0) nanoparticles supported on xonotlite nanowire: a long-lived catalyst for hydrolytic dehydrogenation of ammonia-borane, Dalton Trans. 43 (2014) 1797−1805.

[43] Y. Tonbul, S. Akbayrak, S. Özkar, Nanozirconia supported ruthenium(0) nanoparticles: highly active and reusable catalyst in hydrolytic dehydrogenation of ammonia borane, J. Colloid Interface Sci. 513 (2018) 287−294.

[44] Q.L. Yao, W.M. Shi, G. Feng, Z.H. Lu, X.L. Zhang, D.J Tao, D.J. Kong, Ultrafine Ru nanoparticles embedded in SiO_2 nanospheres: highly efficient catalysts for hydrolytic dehydrogenation of ammonia borane, J. Power Sources 257 (2014) 293−299.

[45] S. Akbayrak, P. Erdek, S. Özkar, Hydroxyapatite supported ruthenium(0) nanoparticles catalyst in hydrolytic dehydrogenation of ammonia borane: insight to the nanoparticles formation and hydrogen evolution kinetics, Appl. Catal. B Environ. 142-143 (2013) 187−195.

[46] L. Wen, J.S. Su, X.J. Wu, P. Cai, W. Luo, G.Z. Cheng, Ruthenium supported on MIL-96: an efficient catalyst for hydrolytic dehydrogenation of ammonia borane for chemical hydrogen storage, Int. J. Hydrogen Energy 39 (2014) 17129−17135.

[47] H. Jia, X.R. Song, S. Liu, X. Xu, X.C. Zheng, Z.K. Peng, P. Liu, Assembly and superior performance of palladium nano-catalysts anchored to a magnetic konjac

glucomannan-graphene oxide hybrid for H_2 generation from ammonia borane, J. Taiwan Inst. Chem. E. 100 (2019) 137–143.

Table 1. The catalytic performance comparison of some Ru-based catalysts for AB hydrolysis.

Catalyst	Ru/AB (mole ratio, × 10^{-3})	TOF ($mL_{H_2} \cdot g_{Ru}^{-1} \cdot min^{-1}$, × 10^3)	E_a (kJ mol^{-1})	Reference
Ru/nanodiamond	3.30	56.2	50.7	[20]
Ru/HfO_2	3.96	41.7	65	[27]
Ru/graphene	10.00	24.5	11.7	[39]
Ru/C	1.78	27.7	76	[41]
Ru/X-NW	2.71	33.1	77	[42]
Ru/ZrO_2	6.30	42.4	58	[43]
Ru@SiO_2	2.50	49.1	38	[44]
Ru/HAp	3.92	33.6	58	[45]
Ru@MIL-96	3.90	56.7	48	[46]
Ru/g-C_3N_4	1.98	122.2	35.6	This work

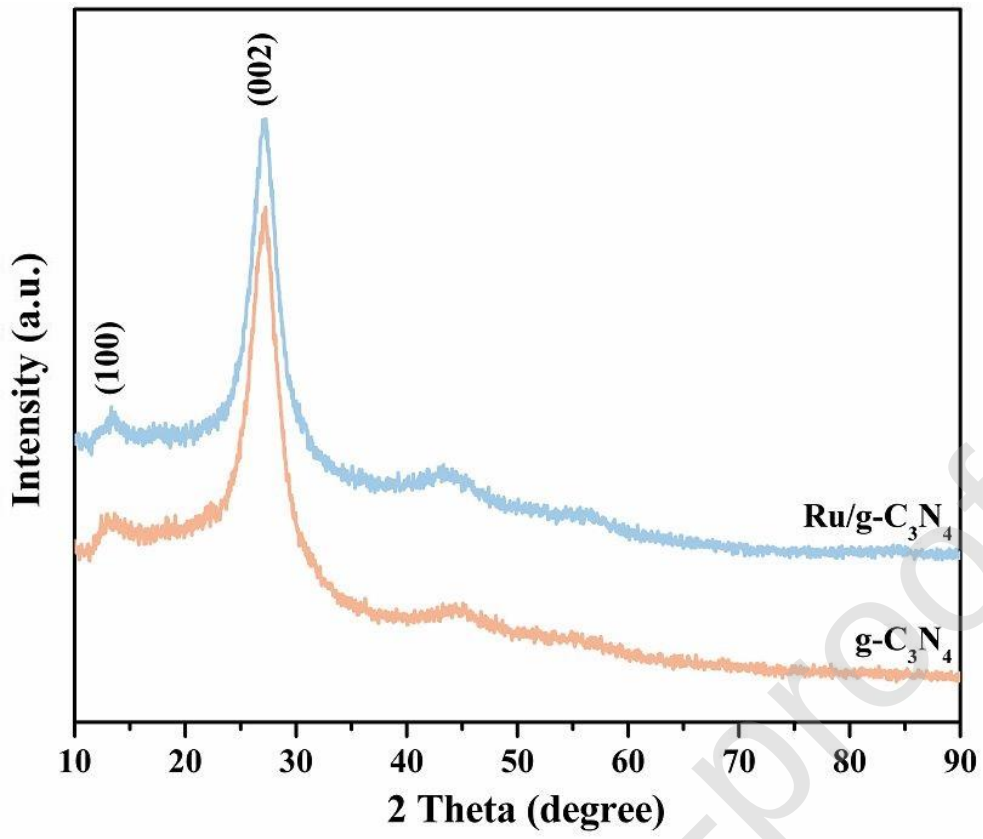

Fig. 1 XRD patterns of g-C_3N_4 and the Ru/g-C_3N_4 porous catalysts.

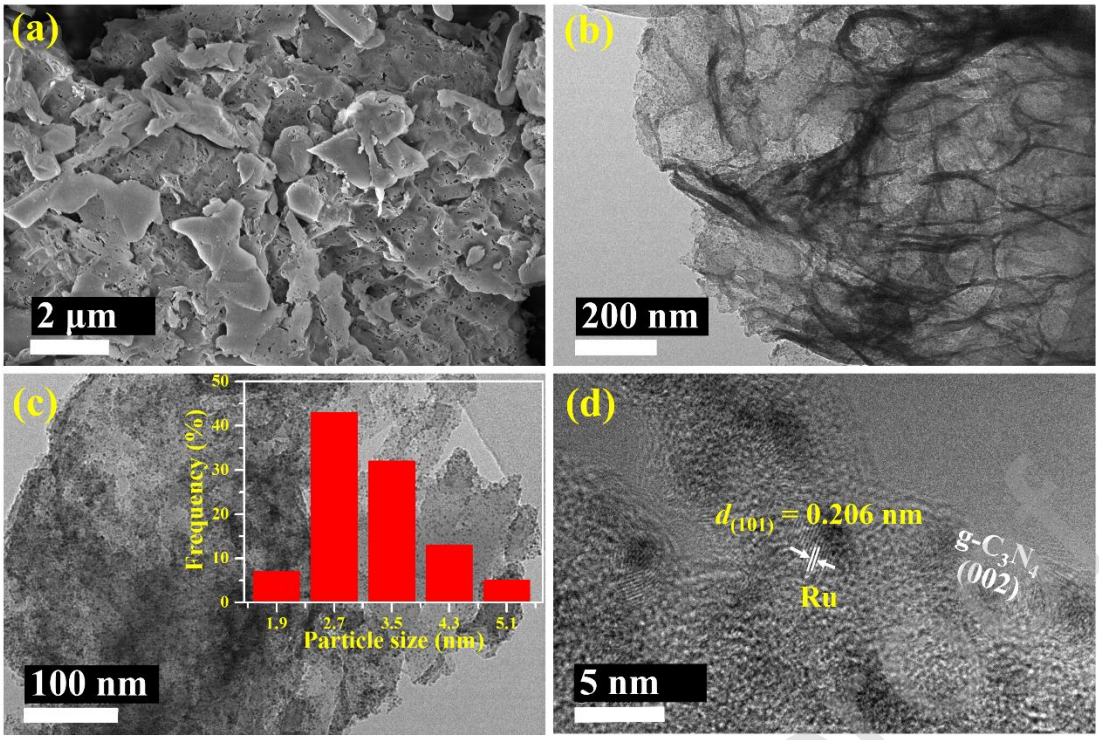

Fig. 2 SEM image (a) TEM images (b, c), HRTEM image (d) of the Ru/g-C_3N_4 porous catalysts, and corresponding particle size distribution of Ru NPs (inset of c).

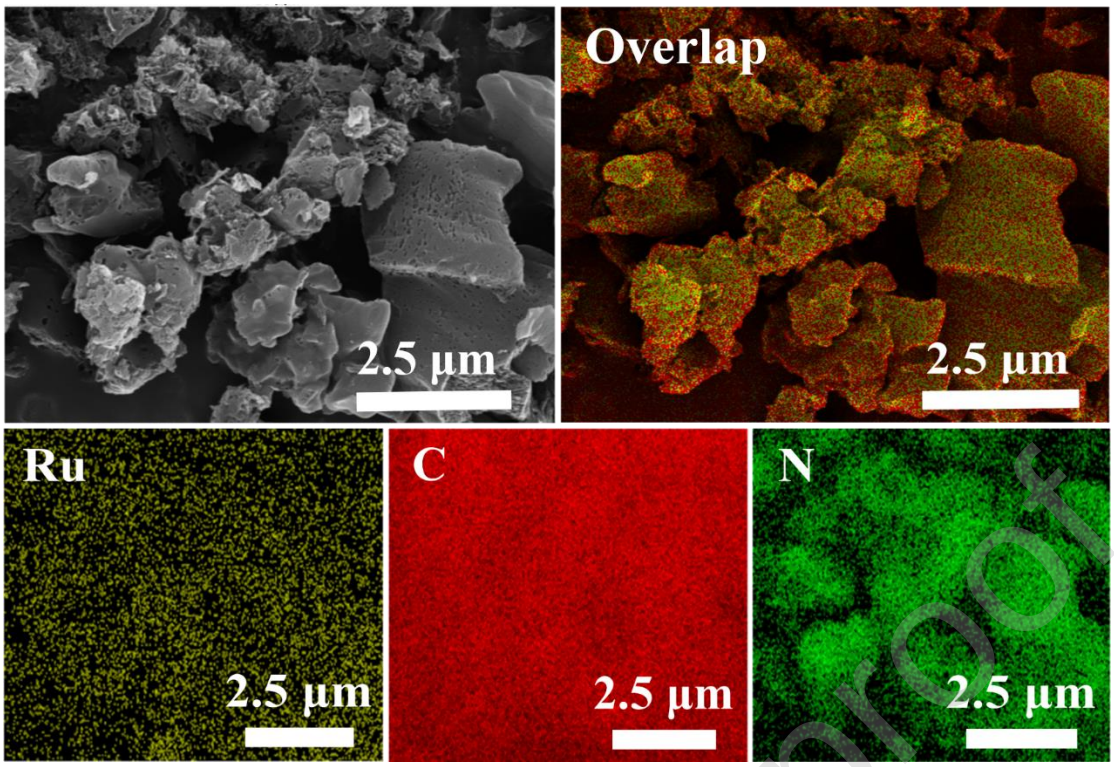

Fig. 3 EDX elemental mapping of the Ru/g-C_3N_4 porous catalysts.

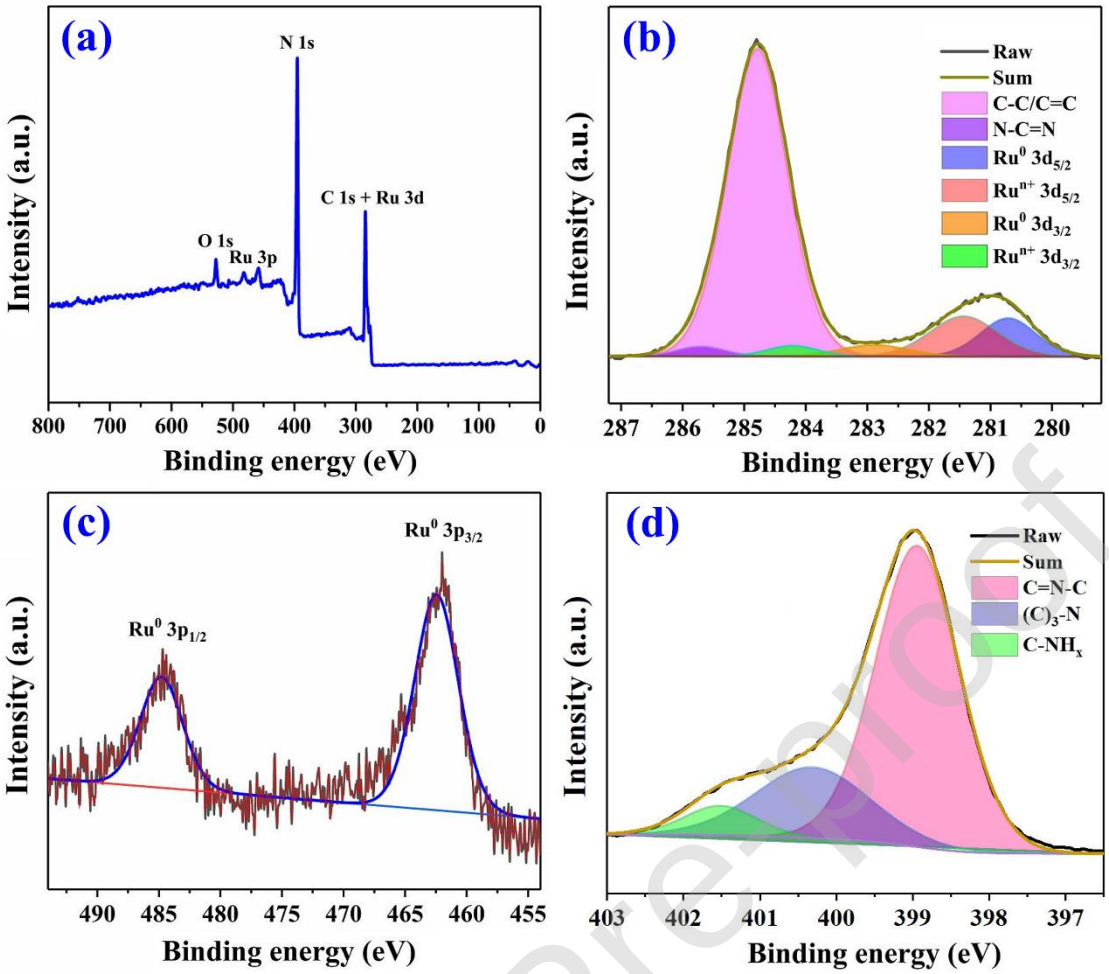

Fig. 4 XPS survey spectrum (a), high-resolution C 1s + Ru 3d (b), Ru 3p (c), and N 1s spectra (d) of the Ru/g-C_3N_4 porous catalysts.

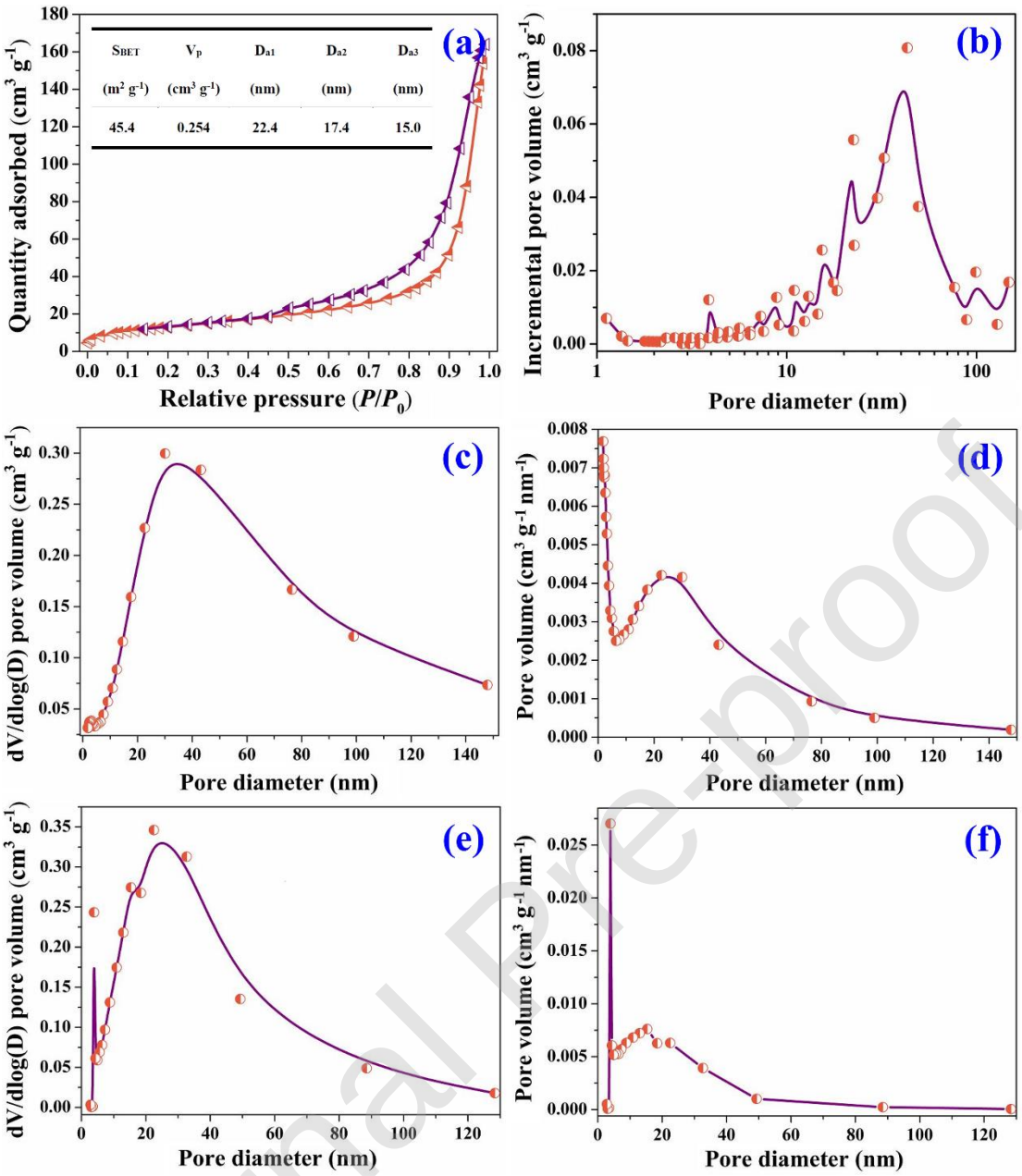

Fig. 5 N_2 adsorption-desorption isotherm (a) and pore size distribution curves of the Ru/g-C_3N_4 porous catalysts (b-f, b: obtained from the desorption branch by the DFT model; c and d: obtained from the adsorption branch by the BJH method; e and f: obtained from the desorption isotherm by the BJH method).

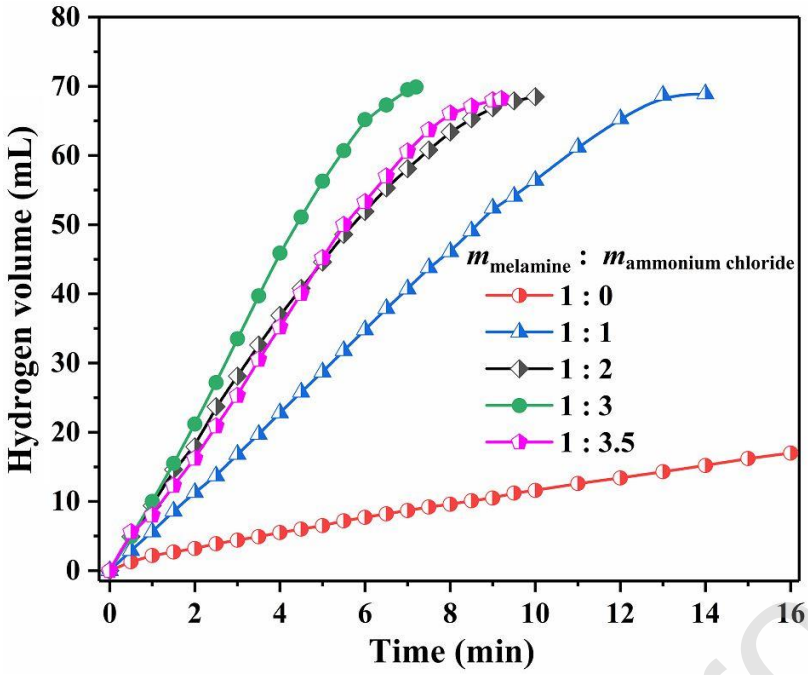

Fig. 6 The influence of different mass ratios of melamine to NH_4Cl on the catalytic activity (with the conditions of catalyst dosage 25.0 mg, AB dosage 31.0 mg, DI water 25.0 mL, and reaction temperature 303 K).

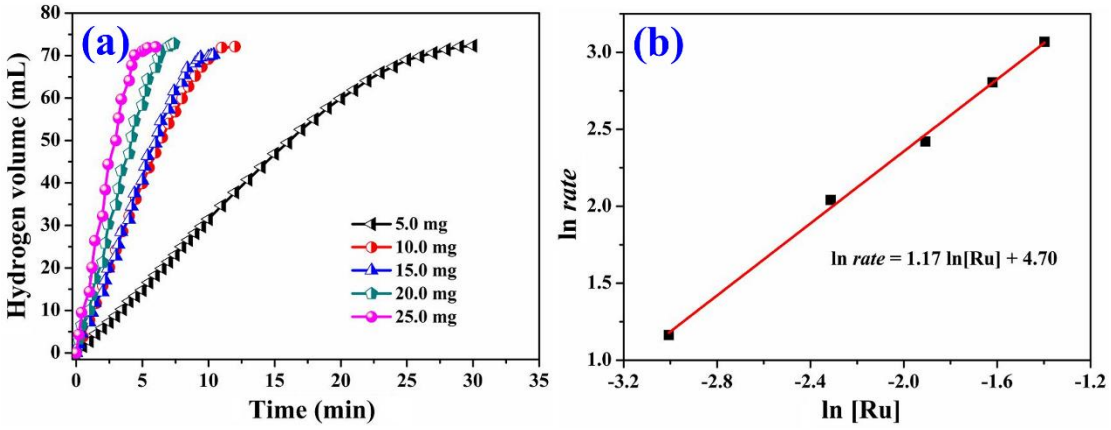

Fig. 7 Hydrogen evolution over the Ru/g-C_3N_4 porous catalysts with different dosages (a) and the corresponding plots of ln *rate* versus ln [Ru] (b) (with the conditions of AB dosage 31.0 mg, DI water 25.0 mL, and reaction temperature 303 K).

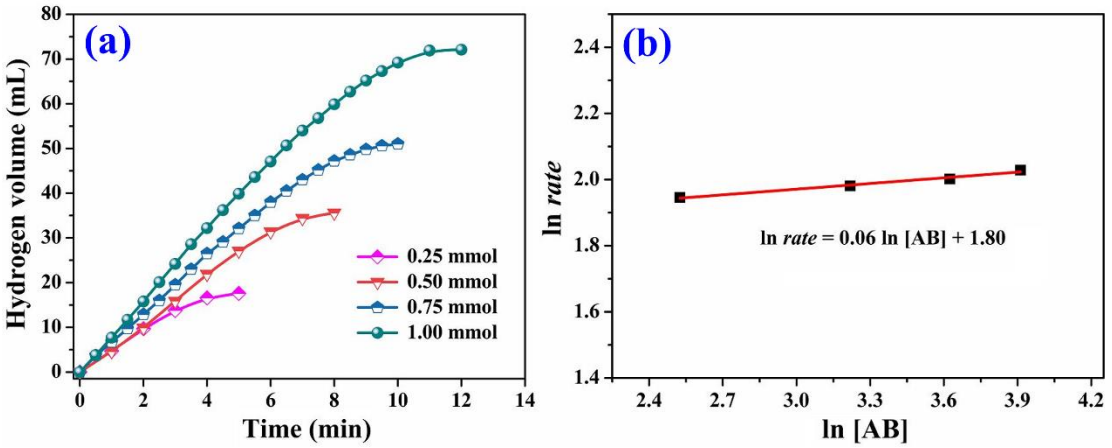

Fig. 8 Hydrogen evolution over the Ru/g-C_3N_4 porous catalysts with different AB dosages (a) and the corresponding plots of ln *rate* versus ln [AB] (b) (with the conditions of catalyst dosage 10.0 mg, DI water 25.0 mL, and reaction temperature 303 K).

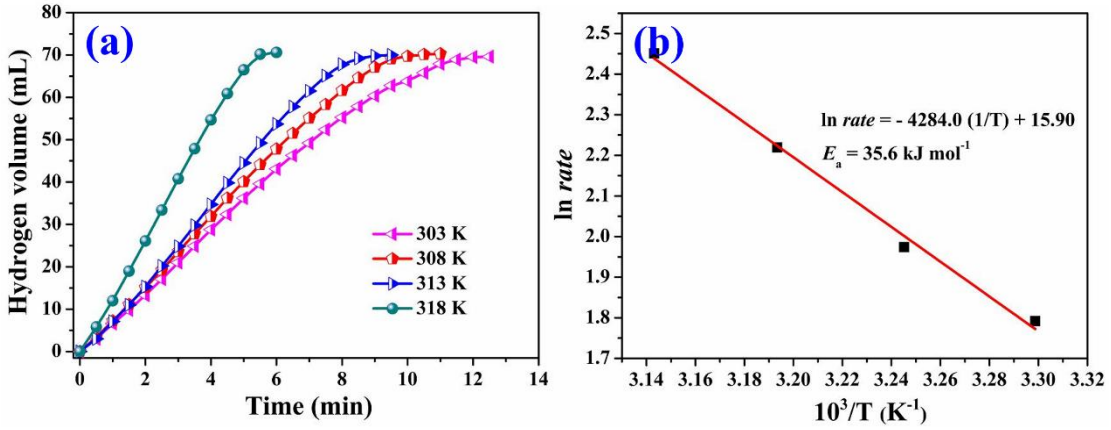

Fig. 9 Hydrogen evolution over the Ru/g-C_3N_4 porous catalysts at different temperatures (a) and the corresponding Arrhenius plots (b) (with the conditions of catalyst dosage 10.0 mg, AB dosage 31.0 mg, and DI water 25.0 mL).

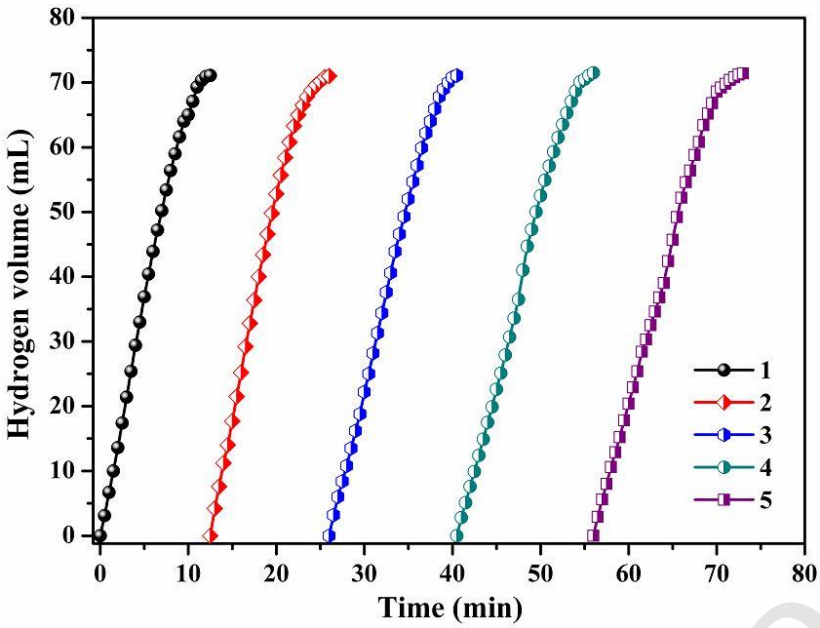

Fig. 10 Recyclability of the Ru/g-C_3N_4 porous catalysts (with the conditions of catalyst dosage 10.0 mg, AB dosage 31.0 mg, DI water 25.0 mL, and reaction temperature 303 K).